Experimental sticking coefficients of CO and N2 on sub-micrometric cosmic grain analogs

C. Stadler, C. Laffon, Ph. Parent

Astronomy & Astrophysics manuscript no. output
July 9, 2024

Experimental sticking coefficients of CO and N_2 on sub-micrometric cosmic grain analogs

C. Stadler[1], C. Laffon[1], and Ph. Parent[1]

Aix Marseille Univ, CNRS, CINaM, Marseille, France
e-mail: caroline.stadler@univ-amu.fr, philippe.parent@univ-amu.fr

July 9, 2024

ABSTRACT

Context. Measuring the sticking coefficient of molecules pertinent to astrochemistry - such as CO - on substrates that mimic interstellar dust grains is crucial for the comprehensive understanding of gas-grain chemical processes. Although astrochemical models assume a sticking coefficient of 1, recent laboratory experiments on H_2O and CO_2 have revealed significantly lower values when measured on small grain analogs. As the effect of grain size on molecular adsorption has been largely ignored to date, further experiments are needed to determine the accretion rates of species known to freeze out on dust grains.
Aims. Our aim is to determine the sticking coefficients of CO and N_2 on sub-micrometric silicate and carbon grains. By quantifying realistic sticking coefficients on these dust grain analogs, we can improve the accuracy of astrochemists' predictions of molecular abundances as affected by gas-grain interactions.
Methods. The molecules of interest were added to various substrates at 10 K in an ultra-high vacuum. The amount of adsorbate that stuck to the substrate was quantified using X-ray photoelectron spectroscopy. These quantities were compared to a reference with a sticking coefficient of 1, allowing the deduction of the sticking coefficient for each substrate.
Results. The average sticking coefficients of CO and N_2 on grain analogs are 0.17 for CO and 0.14 for N_2 on olivine powder, and 0.05 for CO and 0.07 on N_2 on soot, instead of the presumed 1. This is in line with the low values previously reported for H_2O and CO_2.
Conclusions. These laboratory results indicate that CO and N_2, in addition to H_2O and CO_2, also exhibit a low sticking coefficient on dust grain analogs. It is thus necessary to reconsider the interactions between gaseous species and dust particles as a low-efficiency process. This reduction in accretion and reaction rates has important implications for how we understand astrochemistry.

Key words. sticking coefficient – gas-grain adsorption – laboratory astrophysics

1. Introduction

Carbon monoxide (CO) is one of the most important molecules found in space (Öberg & Bergin 2021). It has been studied both in astrophysical laboratory experiments and via observational astronomy, as well as through a myriad of computer models. Its abundance in molecular clouds – outmatched only by H_2 in the gaseous phase and H_2O in the solid phase – highlights its importance in astrochemistry (McClure et al. 2023). It has been shown to play a key role in the evolution of the chemistry of the interstellar medium (ISM) and protoplanetary disks, both in the gas phase and as ice frozen out on dust grains (Powell et al. 2022; Öberg 2016).

The accretion of gaseous species onto interstellar dust grains relies on a parameter known as the sticking coefficient (SC). This value represents the likelihood of a gas-phase atom or molecule sticking to a grain's surface after it collides with it. So far, experimental SC values have been obtained on centimetric flat substrates (metals, carbon, and silicates), dry or covered with water ice, but not on sub-micrometric grains resembling those found in the ISM. With some exceptions (e.g., Chakarov et al. (1995); Dohnálek et al. (2001)) these experimental SCs were consistently measured to be about 1 for H_2O (Brown et al. 1996), CO, N_2, O_2, CH_4 and CO_2 (Bisschop et al. 2006; Fuchs et al. 2006; Acharyya et al. 2007; Noble et al. 2012; He et al. 2016), as well as for H_2 and D_2 at low gas temperatures (Chaabouni et al. 2012). Consequently, this value has been assumed to be 1 for any gas-phase species, notably in astrochemical modeling (Cuppen et al. 2013).

However, these experimental SC values do not faithfully represent the process of adsorption onto the rugged sub-micrometric particles that make up cosmic dust. Recent measurements on cosmic grain analogs have revealed that the SCs of molecular H_2O and CO_2 ices are far lower than the assumed unity (Laffon et al. 2021). In fact, the tendency of small grains to poorly nucleate ice is a long-known phenomenon in the aerosol chemistry of planetary atmospheres. In this field, it is well accepted that the efficiency with which aerosol particles nucleate ice decreases with aerosol particle size, a parameter deemed more important than the aerosol's chemical composition (Dusek et al. 2006). A comprehensive review of more than 160 laboratory studies on heterogeneous ice nucleation onto small particles can be found in Hoose & Möhler (2012). Experiments consistently report that only a fraction of the aerosol particles' surface nucleates ice, which is assumed to be dependent on several surface-related factors, such as defects or crystallographic faces. An illustration of this phenomenon is the direct observation of nonhomogeneous ice nucleation on micrometric mineral particles (Wang et al. 2016). It shows that ice only nucleates on some parts of the particles, with other parts remaining bare. At the nanoscale, quantum modeling also indicates that selective condensation occurs in the concave cavities of small grains and, conversely, is hindered by convex areas (Buch & Czerminski 1991; Buch et al. 1996). Curvature effects on heterogeneous nucleation can also

Article published by EDP Sciences, to be cited as https://doi.org/10.1051/0004-6361/202449167

be modeled from classical nucleation theory and has been found to be important on spherical particles on a quasi-molecular scale (Fletcher 1958; Conrad et al. 2005); nucleation is less favorable on convex surfaces and more favorable on concave surfaces (the Kelvin effect; (Fletcher 1969)). For small particles, molecular-scale morphology is therefore related to their ability to nucleate ice. This effect has also been sporadically evoked in the context of ice condensation in astrophysics (Papoular 2005; Sirono 2011). It is therefore essential to reevaluate the SCs of important astrochemical molecules on realistic grain surfaces in this context.

Lower SCs result in a reduction in the growth of molecular ice layers, as well as a slowing of the chemical processes that convert atomic species into molecular ones under interstellar conditions (Ruffle & Herbst 2002). Furthermore, the precise comprehension of how atoms accrete and diffuse on surfaces is vital for the modeling of these reactions (Herbst & Cuppen 2006; Biham et al. 2001; Cuppen et al. 2017). It is also important to consider the growth of molecular ice on grains in the presence of a preliminary layer of water ice. As demonstrated by Pontoppidan et al. (2003) and widely accepted since, CO freezes out in space onto dust grains coated in layers of water ice. Following this, measurements taken for this study were conducted both on dust analogs that were covered in water ice and "dry" samples, to obtain an understanding of the effect of water ice on the SC of molecules on grains.

The present study builds on that of Laffon et al. (2021), who used X-ray photoelectron spectroscopy (XPS) to measure the growth of CO_2 and H_2O ice layers on various cosmic grain analogs. XPS allows for the quantification of adsorbed molecules independently of the specific surface area of the substrates, which is not possible with other available techniques. This method was used to measure the sticking probability of CO and N_2 on grains, complementing the study of CO_2 and H_2O to determine whether these low SCs are a general phenomenon. While CO was selected due to its abundance and significance in the ISM, N_2 was chosen for the sake of comparison, as it has the same molecular mass as CO but possesses different chemical properties, such as no electric dipole. This allowed the impact of molecular characteristics on the system to be assessed. No dipole moment also implies that N_2 is not directly detected in space, but astrochemical simulations predict that it exists in significant concentrations in ices (Iqbal & Wakelam 2018) and is necessary for the development of observed nitrogenous species, such as NH_3 or HCN.

2. Methods

This study was conducted using the SUrface MOleculaire (SUMO) ultra-high vacuum setup at the Centre Interdisciplinaire de Nanoscience de Marseille (CINaM), at Aix-Marseille Université. The complete methodology has been extensively described within the Supplementary Information of Laffon et al. (2021). In brief, in a first chamber with a base pressure of 1.10^{-10} Torr, molecular vapors are condensed onto a cooled substrate and held on a temperature-controlled closed-circuit cryostat (SHI-APD), with a minimum temperature of 10 K. This chamber includes several microleak valves for the background dosing of CO, N_2, and H_2O gases, a quadrupole mass spectrometer (Hiden) to monitor the pressure of the vapor of the added CO or N_2 within, and a cold cathode ion gun (VG) to clean the surfaces with argon ions before a study. The XPS measurements were carried out in a secondary chamber, composed of an X-ray tube (PSP Vacuum TX400) operated at 100 W and located 7 cm from the sample, and a hemispherical electron analyzer (PSP Vacuum Resolve 120) with a pass energy of 50 eV. The XPS data were recorded at a take-off ("magic") angle of 55 degrees, which allowed a direct comparison of the quantities of a molecule adsorbed on both flat surfaces and grains (Gunter et al. 1997). This second chamber also includes an FTIR setup in a vacuum (JASCO 6300V) with a reflection-absorption geometry, which allowed us to confirm that the SC of CO on Au is 1 (see Appendix A) - a value close to the 0.9 reported using thermal desorption by Bisschop et al. (2006). FTIR was also used to check that only minor amounts of X-ray byproducts were created during the study, as well as to ensure that X-ray photodesorption was negligible during the experiments (Basalgète et al. 2022).

The CO and N_2 samples were added in the gas phase to each substrate maintained at 10 K. Sequential additive gas exposures were required to determine SCs; they were made with partial pressures of 1.10^{-8} Torr during the time necessary to obtain the desired exposure in langmuirs (1L = 1.10^{-6} Torr.sec). Applying the Hertz-Knudsen relationship, which relates molecular flux to gas pressure, 1 langmuir is equivalent to 10^{15} molecules impacting the surface per cm^2 per second, provided that the pressure - as measured by a Bayard-Alpert gauge - is corrected from the ionization coefficient and divided by the square root of the molecular mass of the considered molecules (Schutte et al. 1993). Using the commonly accepted density of surface sites of 10^{15} sites per cm^2 for a monolayer (ML), 1 L of gas exposure leads to a condensed layer of 1 ML for an SC of 1. Hereafter, gas exposure is defined in ML units. The surface coverage values used in Fig. 2 are also in ML units, and are defined as the SC multiplied by the gas exposure. The surface coverage was obtained from the XPS elemental analysis of the surface composition after each gas exposure, which allowed for a comparison of the SC on various substrates. Each successive exposure increased the XPS adsorbate signal, which was compared to the equivalent amount of CO on a gold surface, which has a SC of 1. We assumed that the SC is also 1 for N_2 on gold. This ratio provides the SC for the molecules on the substrate of interest. Further details on the method are given in Appendix A.

The substrates used were (1) a gold foil of 1 cm^2 (99.95%, Alfa Aesar), (2) a cut and polished unoriented olivine crystal of 1 cm^2 (originating from San Carlos), (3) a micrometric olivine obtained after finely grinding the remains of the cut from the same olivine crystal (0.30 ±0.14 μm), and (4) a soot sample made of carbon nanoparticles (0.025 μm) with a graphitic structure (see Appendix B). The gold foil and olivine crystal were affixed with silver paint directly onto the sample holders, while the olivine powder was deposited via drop casting. These sample holders were then affixed to the cold finger to ensure an efficient thermal contact. Before cooling, all surfaces were cleaned with a 5-minute argon ion bombardment at 4 keV, resulting in the loss of their crystallographic order to a depth of around 10 nm for both the carbon soot and the olivine samples, whose surfaces needed to be entirely amorphous. In powdered samples like soot and olivine powder, thermal conduction happens through percolation; the cold temperatures diffuse into the sample from the cold finger it is in contact with. If the sample is too thick, cold conduction within the powder can be slow, leading to a temperature difference between the part of the sample in contact with the cryostat and its surface facing the vacuum. The surface receives thermal energy from the chamber walls, counteracting the cooling process.

For each sample, we ensured that the XPS signal from the substrate completely disappeared at high CO or N_2 exposure. This confirmed that the surface of the grains was covered by the

expected multilayer of CO or N_2, and was correctly cooled to the cryostat temperature. Otherwise, the surface of the grains would be warmer than the cryostat, which could lower the SC (He et al. 2016).

For samples covered with water ice, the H_2O exposure was made at 120 K to form a nonporous amorphous solid water (ASW) layer before being cooled to 10 K. The thickness of this layer was 30 ML on flat substrates and 3 ML on powders, thin enough to conserve their rugged surface morphology. In nonporous solid water films, molecular diffusion is limited (He et al. 2019), and therefore our measurements of the SCs on ice-covered substrates should not be affected much by diffusion into the bulk of the ice layers.

3. Results and discussion

Figure 1 shows the SCs for CO and N_2 adsorbed onto the various substrates, dry and pre-covered with H_2O ice (they are also listed in Table C.1). These SC values are the average of the three to four experimental values obtained for successive gas exposures of ≤ 1 ML. They are presented as a function of the average diameter of the grains, considered as spherical for the sake of simplicity. The blue rectangle labeled "ISM grain size" delimits the typical size range of ISM grains. The SC values were found to be 0.50 for CO and 0.40 for N_2 on the olivine crystal – values that are in agreement with the 0.47 reported for CO on MgO (Dohnálek et al. 2001). It falls to 0.17 for CO and 0.14 for N_2 on the olivine powder, and 0.05 for CO and 0.07 for N_2 on soot. For surfaces covered with nonporous ASW ice layers, the SCs are 0.60 for CO and 0.45 for N_2 on the olivine crystal, 0.13 for CO and 0.17 for N_2 on olivine powder, and 0.10 for CO and 0.09 for N_2 on soot. The SCs are similar when the grains' surfaces are dry or covered in water ice, demonstrating that the chemical composition of the grains' surface has a minimal impact on the adsorption probability. Conversely, on the flat surface of olivine, the nature of the adsorbate modifies the SC value, which is slightly higher for CO than for N_2, as well as slightly higher in the presence of ice. These findings are consistent with the Laffon et al. (2021) study on H_2O and CO_2, comparable in both the measured SC and the idea that there is seemingly no significant connection between the nature of the molecules and the grains' surface chemistry at this scale.

For cosmic dust analogs, the main parameter influencing the SC is, to a first approximation, the size of the grains. The smaller the size of the substrate, the lower the SC. Yet, it is essentially the local morphology - on a molecular scale - that is the most important parameter controlling the SC. For small grains, morphology and size are correlated, since their small size implies the existence of entire sections of their surface with a convex curvature. Due to the Kelvin effect on a molecular scale, these convex areas are places where sticking is naturally weaker than on flat parts and concave surfaces, such as valleys, where condensation occurs preferentially (Fletcher 1958, 1969; Buch & Czerminski 1991; Buch et al. 1996; Grosfils & Lutsko 2021).

Figure 2 presents the evolution of the SCs as a function of the surface coverage of both CO and N_2 on grains. The SCs remain consistently low throughout the entire range of coverages investigated, with some variations. On soot, very little change is observed, while on olivine grains the initial SCs have a higher value before dropping after the coverage of 0.3 ML, for both CO and N_2. As of now, there is a lack of molecular-scale characterizations to explain the detail of these curves; however, in the case of olivine, the first molecules to land on the surface have a higher sticking probability, likely due to a preferred adsorption onto

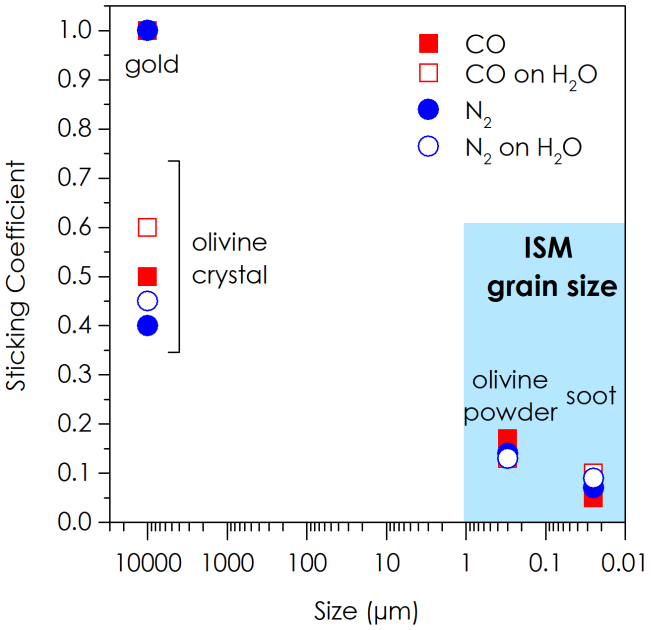

Fig. 1. SCs with respect to substrate size (note the logarithmic scale).

surface defects. These defects are nucleation sites for molecular clusters (Stirniman et al. 1996), which grow from those points to cover parts of the substrate (Wang et al. 2016). The cluster shapes depend on the motion of the adsorbate on the surface and can be simple, such as round islands, or complex, such as fractal frost (Witten & Sander 1981). Adsorption then proceeds on top of or at the edges of these initial clusters, and extends onto the bare surrounding areas, where the adsorption probability is low if the local surface of the substrate is convex or chemically repulsive. The clusters then grow until they cover all parts of the substrate, while the molecular layer develops into the third dimension. In surface science, this is described by the Volmer-Weber growth mode, if the area around the islands remains devoid of molecules, or a Stranski–Krastanov growth mode, if the islands grow on a monolayer (Yu & Thompson 2014; Song et al. 2014). This type of growth has been reported for water adsorption on graphite (Chakarov et al. 1995). For each experiment, no XPS signals from the substrate can be detected around 7 ML, confirming that the whole grain ends up being completely covered by the molecular layers. Yet, the SCs do not reach values close to 1 for CO or N_2 multilayers grown on flat substrates. As the layers studied are very thin, they retain the morphology and hence the curvature of the substrate on which they are deposited. As discussed previously, the morphology of the substrate is the most important parameter controlling the SC, which therefore remains low over the entire range of coverages studied. This also clarifies why pre-coating the grains with an H_2O layer does not significantly raise the SCs: it preserves the morphology of the substrate (i.e. the convex areas), which ultimately keeps the SCs low. Molecular dimensions being very small compared to morphological variations, large thicknesses are required to fill holes and smooth out the grain surface, so the SC is likely to tend toward the values observed on flat substrates (He et al. 2016; Bisschop et al. 2006).

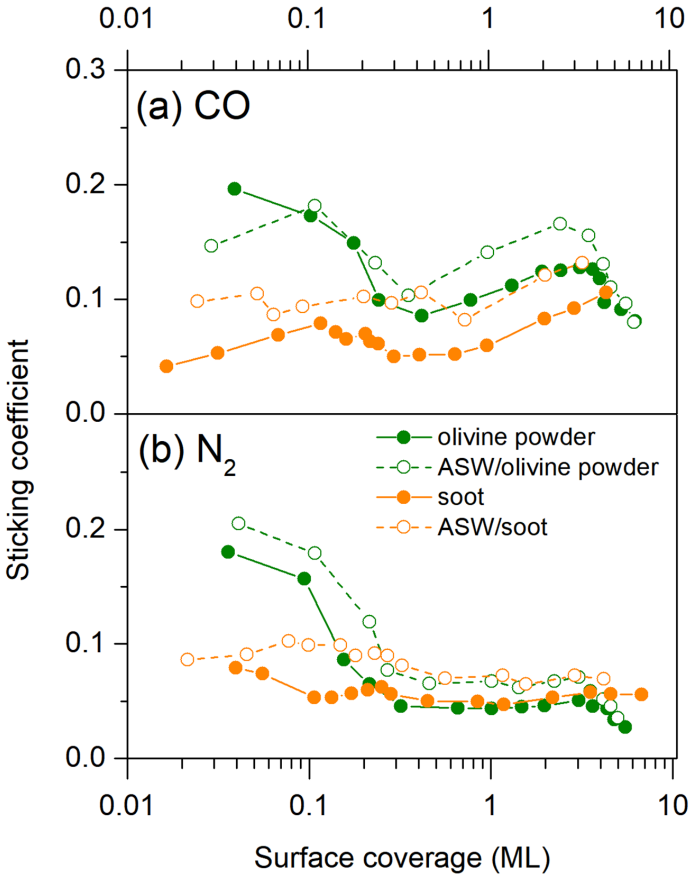

Fig. 2. Evolution of CO (a) and N_2 (b) SCs on different substrates, with coverage (note the logarithmic scale).

4. Conclusion

The SCs on grain substrates are 0.17 for CO and 0.14 for N_2 on the olivine powder, and 0.05 for CO and 0.07 for N_2 on soot. These values are consistent with those found previously for CO_2 and H_2O on the same grain analogs. There is little effect on the SC stemming from the various substrates' chemistries, as shown by similar values between dry and ice-covered grains. Rather, the SC is primarily dependent on the morphology of the substrate itself. For interstellar dust, low SC values will persist until accretion and coagulation processes have increased the radius of their grains. We have also shown that this weak adsorption ability persists even at high surface coverages, indicating that these low SCs should be used not only for first molecular layers, but also for greater thicknesses, until cavities are filled to create a flat surface.

5. Astrophysical implications

In addition to H_2O and CO_2, these findings show that CO and N_2 exhibit a low SC on dust grains. This suggests a universal character of the effect of grain size on condensation, and points to the need to rethink the interactions between gas-phase species and dust grains as a low-efficiency process. The implications of this study are consequential, notably when considering computational astrochemistry. As mentioned, astrochemical models that study gas-grain reactions on the grain surface use an SC of 1 for every molecule, on every surface type. The low measured SCs will reduce both the accretion rate and reaction rates, by several orders of magnitude, changing the time needed for chemical evolution to occur. This change in the kinetics of condensation can be extrapolated from CO and N_2 to atoms such as H, C, O and N, as well as other relevant molecules, if restricted only to physisorption processes. In a chemical kinetics view, the reaction rate is proportional to the molecular concentration of the reactants. So, for a bimolecular reaction, the rate is proportional to the square of the concentration and would therefore be reduced by SC^2. If we consider an average SC of 0.1 per molecule, the rate of bi-atomic reactions A+B will fall by a factor of SC(A) x SC(B), or by 1×10^{-2}, and by a factor of 1×10^{-3} for three-body reactions. Revisiting reaction rates in models that involve gas-grain interactions (Ruaud et al. 2016), but in which SCs are standardized as being 1, is therefore necessary to obtain a more complete image of gas-grain reactions, accretions rates, and gas-solid partitioning below the snow lines. Another astrophysical implication is that sticking on large grains (> 1 µm, like in protoplanetary disks) can be expected to be lower than unity if they are made of agglomerates of small particles (Jones & Ysard 2019), as in this case molecular sticking is controlled by the SC on the primary small particles that make up the larger grain.

Acknowledgements. The authors are grateful for the help of D. Ferry for making these experiments possible, and O. Grauby for his help during sample preparation and SEM imaging. Additionally, thanks are extended to G. Arthaud for his invaluable experimental and engineering support.

References

Acharyya, K., Fuchs, G. W., Fraser, H. J., van Dishoeck, E. F., & Linnartz, H. 2007, A&A, 466, 1005
Basalgète, R., Torres-Díaz, D., Lafosse, A., et al. 2022, J. Chem. Phys., 157, 084308
Biham, O., Furman, I., Pirronello, V., & Vidali, G. 2001, ApJ, 553, 595
Bisschop, S. E., Fraser, H. J., Öberg, K. I., van Dishoeck, E. F., & Schlemmer, S. 2006, A&A, 449, 1297
Brown, D. E., George, S. M., Huang, C., et al. 1996, J. Phys. Chem., 100, 4988
Buch, V. & Czerminski, R. 1991, J. Chem. Phys., 95, 6026
Buch, V., Delzeit, L., Blackledge, C., & Devlin, J. P. 1996, J. Phys. Chem., 100, 3732
Chaabouni, H., Bergeron, H., Baouche, S., et al. 2012, A&A, 538, 1
Chakarov, D., Österlund, L., & Kasemo, B. 1995, Vacuum, 46, 1109
Conrad, P., Ewing, G. E., Karlinsey, R. L., & Sadtchenko, V. 2005, J. Chem. Phys., 122, 064709
Cuppen, H. M., Karssemeijer, L. J., & Lamberts, T. 2013, Chem. Rev., 113, 8840
Cuppen, H. M., Walsh, C., Lamberts, T., et al. 2017, Space. Sci. Rev., 212, 1
Dohnálek, Z., Kimmel, G. A., Joyce, S. A., et al. 2001, J. Phys. Chem. B, 105, 3747
Dusek, U., Frank, G. P., Hildebrandt, L., et al. 2006, Science, 312, 1375
Fletcher, N. H. 1958, J. Chem. Phys., 29, 572
Fletcher, N. H. 1969, J. Atmos. Sci., 31, 1266
Fuchs, G. W., Acharyya, K., Bisschop, S. E., et al. 2006, Faraday Discuss., 133, 331
Grosfils, P. & Lutsko, J. 2021, Crystals, 11, 4
Gunter, P., Gijzeman, O., & Niemantsverdriet, J. 1997, Appl. Surf. Sci., 115, 342
He, J., Acharyya, K., & Vidali, G. 2016, ApJ, 823, 56
He, J., Clements, A. R., Emtiaz, S., et al. 2019, ApJ, 878, 94
Herbst, E. & Cuppen, H. M. 2006, PNAS, 103, 12257
Hoose, C. & Möhler, O. 2012, Atmos. Chem. Phys., 12, 9817
Iqbal, W. & Wakelam, V. 2018, A&A, 615, A20
Jones, A. P. & Ysard, N. 2019, A&A, 627, A38
Laffon, C., Ferry, D., Grauby, O., & Parent, P. 2021, Nat. Astron., 5, 445
McClure, M. K., Rocha, W. R. M., Pontoppidan, K. M., et al. 2023, Nat. Astron., 7, 431
Noble, J. A., Congiu, E., Dulieu, F., & Fraser, H. J. 2012, Mon. Not. R. Astron. Soc., 421, 768
Öberg, K. I. 2016, Chem. Rev., 116, 9631
Öberg, K. I. & Bergin, E. A. 2021, Phys. Rep., 893, 1
Papoular, R. 2005, MNRAS, 632, 489
Pontoppidan, K. M., Fraser, H. J., Dartois, E., et al. 2003, A&A, 408, 981
Powell, D., Gao, P., Murray-Clay, R., & Zhang, X. 2022, Nat. Astron., 6, 1147
Ruaud, M., Wakelam, V., & Hersant, F. 2016, MNRAS, 459, 3756
Ruffle, D. P. & Herbst, E. 2002, MNRAS, 319, 837
Schutte, W., Allamandola, L., & Sandford, S. 1993, Icarus, 104, 118

373 Sirono, S. 2011, ApJ, 735, 131
374 Song, J., Li, Q., Wang, X., et al. 2014, Nat. Comm., 5, 4837
375 Stirniman, M. J., Huang, C., Scott Smith, R., Joyce, S. A., & Kay, B. D. 1996, J.
376 Chem. Phys., 105, 1295
377 Wagner, C. 1983, J. Elect. Spec. Relat. Phen., 32, 99
378 Wang, B., Knopf, D. A., China, S., et al. 2016, PCCP, 18, 29721
379 Witten, T. A. & Sander, L. M. 1981, Phys. Rev. Lett., 47, 1400
380 Yu, H. Z. & Thompson, C. V. 2014, Acta Mater., 67, 189

381

Appendix A: Methods: Additional information

Figure A1 presents the process of obtaining the SCs (SC) from XPS data of CO on carbon nanoparticles (soot). Initially, the CO adsorption on a gold foil serves as a reference. The XPS spectra in Figure A1(a) and A1(b) show the C1s and Au 4f lines for CO on gold, respectively, at 0.0 ML (bare surface) and, as an example, at 0.8 ML CO exposure. At 0.0 ML, the C1s peak at 284 eV results from small amounts of carbon contamination of the gold foil. At 0.8 ML, the CO peak at around 290 eV indicates CO adsorption on the gold foil. Concurrently, the C1s peak at 284 eV diminishes slightly due to the CO adlayer. The Au 4f lines also slightly decrease after 0.8 ML of CO exposure. CO deposition on the gold foil is simultaneously monitored with FTIR in reflection absorption mode, using the intensity of the CO stretching band at 2142 cm^{-1} converted to ML, using the band strength of $1.1x10^{-17}$ $cm.molecule^{-1}$ and the conversion factor 1 ML= 10^{15} $molecules.cm^{-2}$. Figure A1(c) illustrates the deposited CO layers in ML calculated from FTIR as a function of exposure, determined by both the dosing time and collision rate. Figure A1(c) shows that the amount of CO condensed on gold matches the CO exposure in the gas phase (points align on the diagonal line). This indicates an SC=1 for CO on gold.

Figure A1(d) presents the XPS spectra of CO adsorption on carbon nanoparticles (soot), at 0.0 ML and 12.5 ML exposures. The signal from the adsorbate appears as a peak labeled "CO" at around 290 eV, while the C1s peak of the soot substrate is at 284 eV and decreases after the exposure of 12.5 ML of CO. To ensure that the amount of CO deposited on a rugged substrate (such as soot) is comparable to that deposited on a flat substrate (gold foil), data must be recorded at the 55° take-off "magic" angle. To obtain the SC of CO on soot, we proceed as follows. The amount of adsorbate atoms deposited per surface unit is obtained by summing the intensities of all relevant emission lines of the adsorbate, such as the C1s and O1s lines of CO, and dividing by the emission line intensities of all the atoms (adsorbate plus substrate); all lines being corrected for their respective relative sensitivity factors (RSFs). Surface RSFs were used below one ML coverage, and bulk RSFs beyond (Wagner 1983). This ratio allows us to get rid of the surface area and electron shadowing effects intrinsic to the photoemission process of rough surfaces, and thus represents the adsorbate coverage of the substrate per unit surface area.

This ratio is plotted in Figure A1(e) for CO on gold and soot substrates. CO coverage increases more slowly on soot than on gold, indicating a lower SC. To determine the SC on soot precisely, a graphical method is used. For a specific adsorbate fraction, such as 45% (point 1), a horizontal (green) line is drawn to find the corresponding CO exposures for both gold (red) and soot (blue) substrates; in this case 0.83 ML on gold and 12.5 ML on soot. The SC of CO on soot was then calculated by dividing the CO exposure on gold (point 2) by the CO exposure on soot (point 3), which is 0.83/12.5=0.066 in this example.

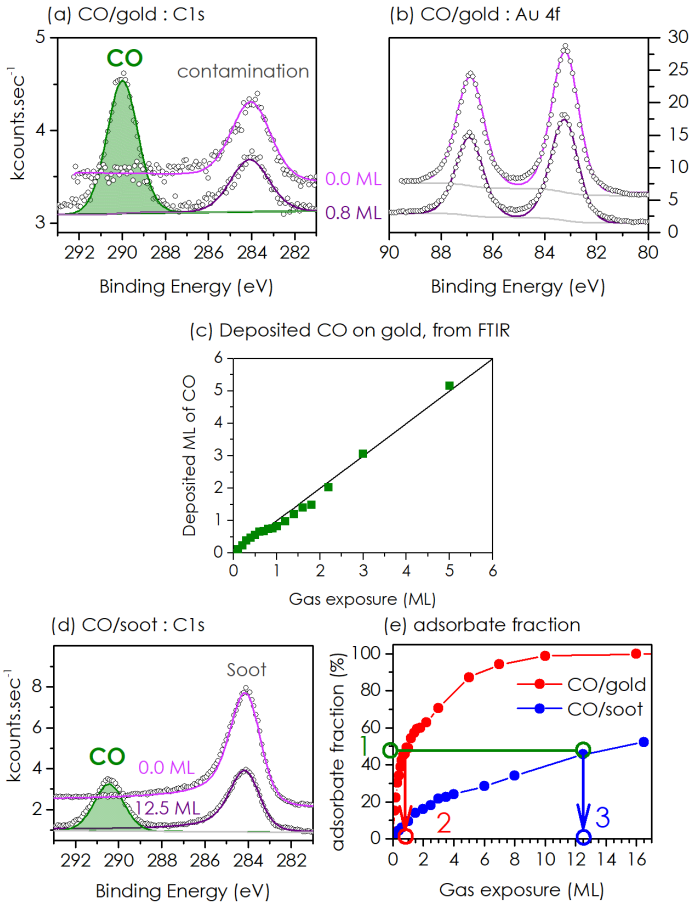

Fig. A1: Data analysis. (a) XPS C1s and (b) XPS Au 4f data for CO adsorbed on gold at 10 K, at 0.0 ML and 0.8 ML of CO exposure. (c) Number of CO layers deposited on gold as a function of CO exposure, deduced from the infrared strength of the stretching CO band at 2142 cm^{-1}. IR intensities follow the diagonal line when SC=1. (d) C1s XPS data for CO adsorbed on soot at 10 K, at 0.0 ML and 12.5 ML of CO exposure. (e) CO coverage per unit surface area (in percent) deduced from the XPS signals (see the main text) as function of the CO exposure. The graphical method for determining the SC of CO on soot consists in dividing the exposure on gold (point 2) by the exposure on soot (point 3) necessary to obtain the same coverage (point 1; see the main text).

Appendix B: Scanning electron microscopy of soot and powdered olivine samples

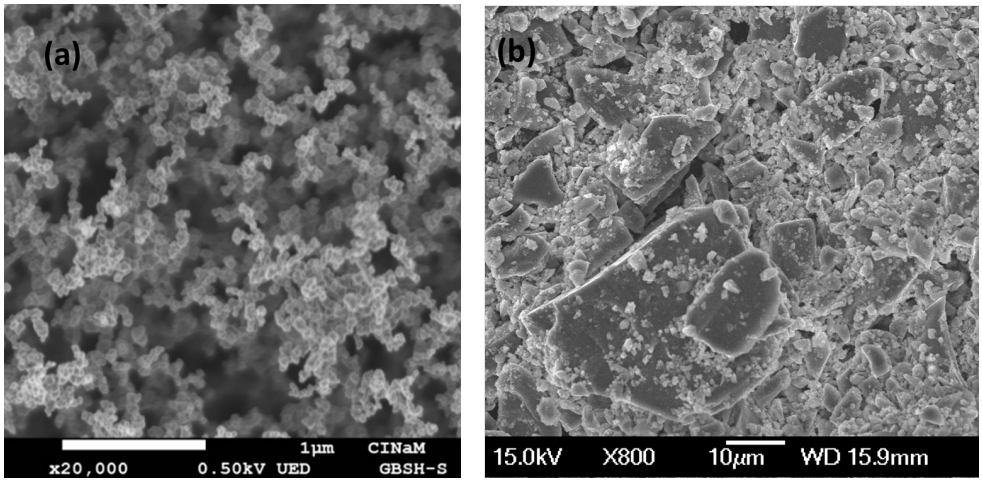

Fig. B1. Scanning electron microscopy images of the soot (a) and powder of olivine (b) samples.

Figure B1 displays scanning electron microscopy (SEM) images of soot (a) and powdered olivine samples (b). Particle size distributions were determined from those images using ImageJ v1.53, an open-source image processing software. The soot sample is made of fractal assemblies of small primary carbon particles (diameter 0.025 µm). The powdered olivine, resulting from grinding olivine crystals, consists of irregular grains and platelets with an average equivalent diameter of 0.30 ±0.14 µm. In Figure B1(b), small grains and platelets mostly cover larger platelets, shaping the powder's morphology onto which CO adsorbs.

Appendix C

Table C.1. Sticking Coefficient per condition

Substrate	CO	N_2	H_2O*	CO_2*
Dry				
Gold	1 ± 0.07	1 ± 0.07	1 ± 0.07	1 ± 0.07
Olivine Crystal	0.50 ± 0.07	0.40 ± 0.07	0.65 ± 0.07	0.42 ± 0.07
Olivine Powder	0.17 ± 0.02	0.14 ± 0.03	0.15 ± 0.01	0.06 ± 0.01
Carbon Nanoparticles	0.05 ± 0.02	0.07 ± 0.02	0.09 ± 0.01	0.04 ± 0.003
On non-porous ASW				
Olivine Crystal	0.60 ± 0.11	0.45 ± 0.07	–	–
Olivine Powder	0.13 ± 0.02	0.17 ± 0.04	–	–
Carbon Nanoparticles	0.10 ± 0.02	0.09 ± 0.03	–	0.04 ± 0.003

Notes. Mean SCs per molecule and substrate. The SC values are the average of the experimental values found under 1 ML of gas exposures. *Results and SC estimated errors from Laffon et al. (2021)